27355 DUP

IGM87D-404-514-G
CNRC 27355

On-line electro-optical instrumentation for continuous quality control of manufactured sheets

by P. Cielo, M. Lamontagne and G. Vaudreuil
Industrial Materials Research Institute
National Research Council Canada
Boucherville, Québec J4B 6Y4 Canada

ABSTRACT

The electro-optical approach is particularly promising for on-line sensing of process-relevant product properties. Recent technological advances in video and optical communication technology have spurred the development of rugged, compact and inexpensive optical components which are particularly suited to noncontact operation in hostile industrial environments. In this paper we shall describe a number of electro-optical techniques which have been developed at our Institute over the last years for the in-process inspection of metallic or polymeric thin sheet products. Examples will include infrared spectroscopic three-wavelength sensing for polyethylene-film thickness monitoring independently of the presence of colored pigments, galvanized-sheet surface finish analysis by time-resolved light scattering as well as coating thickness control by triangulation-based optical monitoring of sheet wobbling.

INTRODUCTION

The accelerated industrial trend toward factory automation and computer-integrated manufacturing is creating an urgent need for on-line sensors to continuously monitor the relevant production parameters. Optical sensors are ideal candidates for such harsh environment applications because of their noncontact nature and of the recent availability of increasingly reliable, inexpensive, compact and rugged optoelectronic devices.

On-line inspection constitutes a sizeable fraction of the production activities. It has recently been estimated[1] that inspection-related tasks are performed by 10 percent of the total work force. In some cases, as in the safety-sensitive area of aircraft fabrication, quality control as a whole may account for up to 60 percent of the product costs[2].

Optical sensors for industrial inspection span a range much wider than the classical visual perception function[3]. Examples are optical nondestructive-testing methods using holographic, speckle, interferometric or thermographic techniques for the detection of subsurface defects by the monitoring of abnormal strain behaviour or thermal propagation, as well as a number of process analyzers such as paper-sheet opacity sensors, fiber-optic pH-monitoring devices, or chemical on-line analyzers using the spectroscopic approach[4,5]. Some recent developments in the visual as well as nonvisual optical sensing field at our institute are described in this paper.

THICKNESS MONITORING OF POLYETHYLENE SHEETS

The thickness inspection of thin organic sheets, such as extruded polymeric sheets or blown-film polyethylene materials, is a problem of great concern for the plastics and rubber industry. A precise machine-direction thickness control is an important requirement for material savings considerations. Moreover, a departure from a uniform cross-machine-direction thickness profile indicates the presence of a process malfunction such as roller misalignment or an eccentricity of the concentric extruding dies in a film-blowing machine. A view of a polyethylene film blowing extruder with the IMRI thickness monitoring prototype installed for double-thickness measurement of the folded cylindrical plastics film is shown in Fig. 1.

Although a wide variety of physical approaches are possible for thickness measurement, (see, e.g., ref. 6, section 7-4), including electric capacitance, microwave attenuation, ultrasonic pulse-echo, thermal response time monitoring, etc., the most widely-used methods for thickness measurement of thin plastic films are nuclear and infrared techniques. Nuclear

sensors of the gamma-backscattering type can inspect plastic sheets of 5 μm to 100 μm in thickness, while higher-power X-ray transmission devices can be used for thicker sheets. Such instruments are, however, relatively expensive and have a number of limitations: they require frequent recalibration, must be installed in close proximity to the film, have a relatively slow response time, which is normally inadequate for machine-direction thickness fluctuation monitoring, and must be handled with care because of radiation hazards.

Infrared techniques[7,8] are increasingly used for monitoring the thickness of transparent films. Two typical configurations are shown in Fig. 2. In both diagrams, a light beam is transmitted through the film. A similar configuration is used in reflection for monitoring the thickness of coatings on opaque substrates. The spectral distribution of the light transmitted through the film is given by the Lambert Absorption Law:

$$(1) \qquad T(\lambda)/T_o = \exp\,[-k(\lambda) \cdot d]$$

where $k(\lambda)$ is the absorption coefficient in cm^{-1} and d is the film thickness in cm, $T(\lambda)$ is the transmitted intensity at the wavelength λ, and T_o is the intensity transmitted in a spectral region where there is no appreciable absorption (although Fresnel reflection losses may occur). The absorbance of the film is defined as:

$$(2) \qquad A(\lambda) = -\log_{10}\,[T(\lambda)/T_o] = 0.4343 \cdot k(\lambda) \cdot d$$

From a measurement of the transmittance $T(\lambda)/T_o$ at the chosen wavelength, one can then evaluate the absorbance and thus the thickness from equation (2) after the factor $k(\lambda)$ has been determined from a calibration with samples of known thickness. It should be emphasized that such a ratio measurement is unaffected by common-noise effects such as source aging or dirt accumulation.

Figure 3 shows the transmittance spectrum of a moderately-dyed, 15 μm-thick polyethylene film[9]. Absorption regions are clearly seen around 4200, 2900, 1420 and 730 cm^{-1} which are characteristic of the polyethylene molecular-vibration bands. By choosing as T_o and $T(\lambda)$ the transmittance values at about 2.1 μm (4750 cm^{-1}) and 2.35 μm (4250 cm^{-1}), the absorbance and thus the thickness can be evaluated with rugged low-wavelength detectors and without being affected by the 1.9 μm and 2.7 μm moist-air absorption bands (see Fig. 4). The presence of strong film pigmentation usually affects only moderately the IR transmission spectrum.

One of the problems encountered with films containing a large amount of light-scattering pigments or having a relatively rough surface finish is the wavelength dependence of the scattering-related attenuation in the transmitted or reflected light beam. As shown in Fig. 5, scattering losses are higher at low wavelengths when a large amount of pigment is present in the film. This behaviour is similar to scattering losses by surface irregularities of root-mean-square roughness R_q much smaller than the wavelength: in such a case it can be shown[13] that the specular reflectance from the rough surface has a spectral distribution:

$$(3) \qquad r(\lambda) = r_o \exp\,\{-(4\,\pi\,R_q\,\cos\theta/\lambda)^2\}$$

where r_o is the light intensity reflected by a perfectly smooth mirror and θ is the angle of incidence. The dependence of the scattering losses upon the light wavelength is strikingly apparent in Fig. 6, showing the transmittance spectrum of a heavily pigmented, black-carbon-filled film. If the thickness is evaluated by simply taking the ratio between the transmittivities at, e.g., 2.1 μm and 2.35 μm, Figs. 5 and 6 shows that the estimated value will be smaller than the real value when the scattering-related attenuation is of the same order of magnitude as the absorption-related attenuation. Better thickness evaluation can be obtained independently of the scattering level by measuring the transmittance at three wavelengths, e.g. 2.05 μm, 2.2 μm and 2.35 μm, and using the two signals detected at the lower wavelengths to extrapolate the transmittance without absorption at 2.35 μm, as shown by the dotted lines in Figure 5. By applying the three-wavelength method (Fig. 7), the measured absorbance at 2.35 μm became linearly related to the film thickness as implied by equation (2). Such a technique gives a much better precision while making the measurement independent of the scattering properties of the inspected material.

Another example of the accuracy which can be obtained with the three-wavelength thickness monitoring sensor is given in Table 1. In this case a polyethylene-acrylic copolymer coating was monitored in reflection using an apparatus of the kind shown in Fig. 8. Although the coating was essentially clear, wavelength-dependent scattering may occur in this case mainly because of the random surface profile of the aluminum foil. The results are in agreement with the manual verification (performed by peeling off the film after chemical etching and weighing it - a rather laborious procedure) within a few percent

points. It should be mentioned that the spinning wheel approach shown in Fig. 8 proved adequate for the inspection of stationary samples; for on-line gauging on the moving film, the multiple-detector approach shown in Fig. 2a was preferred because the same portion of the film is inspected simultaneously in this case, giving more reliable measurements for the films whose thickness fluctuates significantly in the machine direction.

Table 1 Optical measurements vs. weighed values for the thickness of a plastics coating on aluminum foil (A: optical measurement; B: weighed data)

A	B	A	B	A	B
32.2	32.0	30.6	32.1	32.0	30.1
32.3	32.5	32.1	32.4	30.0	29.9
30.9	30.2	34.1	32.1	33.1	32.3
33.0	31.3	33.2	31.9	33.6	32.6
30.1	28.8	33.0	32.6	32.6	32.2
31.2	30.8	31.6	30.9	31.7	31.4
33.0	31.3	35.7	36.4	34.7	32.5
33.5	32.2	35.0	33.9	37.1	36.1
32.4	32.2	35.8	34.3	35.0	33.0
32.2	31.5	35.1	34.4	34.6	33.8

INTERFERENCE FRINGE ANALYSIS

Figure 3 also shows the presence in the 2800 to 1000 cm^{-1} spectral region of some interference fringes due to multiple reflections within the film. Such fringes are particularly evident in the longer-wavelength spectral region where the surface-roughness amplitude becomes small with respect to the optical wavelength. The contrast and position of the fringes is also dependent on the angle of incidence and on the angular aperture of the inspecting device. For smoother films, the presence of fringes in the low-wavelength region is a major cause of noise in the evaluation of the absorption-peak depth. Several methods can be used to minimize the interference fringes[10], such as using larger angular apertures or oblique angles of incidence superposing both the transmitted and reflected light beams which have reversed fringe patterns. Another approach is to use the fringe information to better estimate the film thickness from the expression[20]:

$$d = 1/[2\Delta\nu\,(n^2 - \sin^2\theta)^{\frac{1}{2}}] \qquad (4)$$

where $\Delta\nu$ is the interference-fringe separation in cm^{-1}, n is the refractive index of the film material and θ is the angle of incidence. The fringe visibility can be improved by properly processing spectrograms obtained separately with light polarized in the two normal planes.

Such an approach will now be illustrated with reference to a coating inspection problem. Plastic-coated steel sheets were to be inspected for coating thickness by a magnetic-steel manufacturer. A feasibility study using the spectral approach in reflection was performed at our institute on samples with coating thickness ranging from 2.5 to 5 μm using an FTIR spectrometer. A typical spectral distribution of the light reflected from the coated-steel surface is shown in Fig. 9. This spectrum is difficult to interpret because of the presence of multiple-reflection interference fringes which interfere with the absorption peaks, as well as of a number of distortions related to instrumental parameters such as the spectral-radiance curve of the source, the spectral sensitivity of the detector and the presence of absorption bands from water vapor and carbon dioxide in the atmosphere.

The signal fluctuations produced by the interference fringes can be separated from the other features of the spectrum by operating in polarized-light conditions near the Brewster angle of incidence (nearly 50 degrees, see Fig. 10). Figure 11 shows the normalized spectra obtained in the same conditions as in Fig. 9 but with a polarizer inserted across the light beam so that the polarization vector was (a) perpendicular (S-polarization), and (b) parallel (P-polarization) to the plane of incidence. In the S-polarization case, Fig. 11a, the reflection at the coating-to-steel interface interferes with a strong air-to-coating reflection to produce a high-contrast interference-fringe pattern. In the P-polarization case, Fig. 11b, no reflection takes place at the air-to-coating interface at the Brewster angle, so that no interference fringes are present. The film thickness can thus be reliably

evaluated by measuring the interfringe from the S-polarized spectrum and applying equation (4), or else by measuring the absorbance in the 2900 cm^{-1} absorption of the P-polarized spectrum band and evaluating the thickness from equation (2).

SURFACE ROUGHNESS ANALYSIS OF GALVANIZED-STEEL SHEETS

Hot-dip galvanized steel is an economically important product for the steel industry. On-line surface quality sensors would be welcome in this field in order to minimize retreatment costs. Moreover, if a suitable quality-assurance program could be established, the market potential for such a product could be much more extensive, including the automotive-manufacturing applications.

One of the critical parameters of galvanized steel for the applications requiring acceptable aestetic properties, such as external body-walls in automotive applications, is the quality of surface finish. Large-crystal spangle patterns on the hot-dip zinc coating affect the visual surface smoothness even after painting. Different processing techniques are used for spangle grain reduction such as the Heurtey particle-seeding process or surface uniformization by temper-rolling.

Fig. 12 shows the surface texture characteristics of (a) a conventional galvanized-steel sample, (b) a sample with minimized spangle (surface grain size of the order of 1 mm) and (c) a galvanized and matt-finish temper rolled sample with grain boundaries still visible. A systematic study of the possibilities offered by optical technology for the noncontact characterization of this kind of surface was performed at our institute[11]. This paper will focus on the time-resolved light scattering approach.

The light scattering method[12] has been widely applied to the surface roughness analysis both in the laboratory[13,14] and in the production line[15,16]. The basic principle is shown in Fig. 13. When a collimated light beam is incident on a rough surface, the angular spectrum of the scattered light has a maximum at the specular direction. Depending on the ratio of the r.m.s. roughness amplitude R_q to the light wavelength λ, the physical mechanism which determines the angular distribution of the scattered light is either diffraction or geometrical reflection. When R_q is much larger than λ, as it is normally the case when steel-sheet surfaces are inspected with a visible wavelength, the angular spectrum of the scattered light is mainly related to the average surface slope across the illuminated surface. If a correlation can be established between the surface characteristics of interest to the process engineer and the features of the angular spectrum of the scattered light, such an analysis can be used as a powerful in-process tool for quality control[15,16]. This approach is quite attractive for on-line applications for a number of reasons: (1) it has both high sensitivity and large depth of field because it does not require fine focusing as it is the case of triangulation-based or camera-imaging methods; (2) the instrumentation is noninvasive in the sense that it is noncontact and can be located at a safe distance from the inspected workpiece. This is particularly convenient when inspecting high-temperature sheets which may be subject to important vertical fluctuations; (3) the scattered light contains simultaneous information on the surface features of the whole illuminated area. Statistically-significant data can thus be collected at a much faster pace than with line-profilometers.

A number of typical light-scattering angular patterns recorded for samples at different finish properties under He-Ne laser illumination are shown in Fig. 16. Most of the unrolled samples, such as samples Nr. 1, 2, 5 and 6 had a similar angular spectrum when the illuminated area comprised several spangle grains. Minimized-spangle sample Nr. 7 had a somewhat lustrous surface appearance, which is responsible for the more pronounced central peak in the corresponding semi-log curve in Fig. 14. The angular pattern obtained with the temper-rolled samples Nr. 3 and 4 is much broader, in accordance with its matt-finish appearance. Such a light-scattering component for matt-finish surfaces could be substantially eliminated by using a CO_2 laser source whose wavelength is much larger than the R_q surface roughness[11].

A different approach consists in recording a time-resolved signal of the scattered light while the galvanized sheet is moving under the moderately focused laser beam. In most of the previous literature reviewed above, the laser surface-scatter characteristics were analyzed over a relatively large illuminated area to provide an average angular pattern over a large number of spangle grains. On the other hand, local reflectivity variations from grain to grain may be put in evidence, if the laser beam is focused on a small area of the moving sheet surface. Such variations are very useful in the evaluation of the spangle grain size, which is difficult to determine from a comparison of the average angular-scatter pattern.

The variation of the scattering characteristics from grain to grain is clearly apparent from the shape of the scattered beam. Fig. 15 shows the light pattern scattered by (a) a shiny grain, (b) a matt-looking grain, and (c) a boundary region (showing the highly directional scatter patterns from three intersecting grain boundaries) when a conventional large-spangle surface is illuminated by a He-Ne laser of 1 mm^2 cross-section. Clearly, the angular characteristics of the scatter pattern are quite different from grain to grain, depending on the relative orientation of the crystal axes in each grain with respect to the surface. The angular profiles of the scattered field (shown in Fig. 16) for a shiny (curve 1a) and matt (curve 1b) grain confirm such qualitative considerations.

Strong variations in the specular reflectivity (or in the ratio between the reflectivities at two different angles) of a sheet surface moving under a focused light beam are thus observed from grain to grain. The time frequency of the detected signal can be related to the average grain size if the sheet velocity is known. This was verified with an experimental setup using a He-Ne beam relatively well focused on the side-moving surface (waist diameter of the order of 100 μm, depth of field of a few centimeters) while the specularly-reflected light was collected by a variable-aperture detector. A sample with variable spangle grain size sample was first analyzed with such an apparatus. The results are shown in Fig. 17. The top signal was obtained with a spangle grain size of the order of 1 mm, while the bottom signal was obtained, at the same speed, with a spangle size of nearly 3 mm. The frequency difference obtained with these two samples is quite apparent.

OPTOELECTRONIC RANGING OF THE GALVANIZED STEEL SHEET

Range monitoring by noncontact distance measurement is required in a large number of industrial seccors. Examples are robot-to-workpiece positioning[17], flatness control of rolled metal sheets[18], automated focussing of cameras[19], etc. For many industrial applications, the range-sensing device must be compact, it must be suitable for operation under hostile environmental conditions such as high temperatures, presence of fumes, mechanical shocks and large vibration amplitudes, it must have high sensitivity while operating over a relatively long range in order to accommodate wide transverse fluctuations of the workpiece with minimum repositioning requirements, it should operate on materials of widely variable surface conditions, and in most cases it must be inexpensive both in terms of installation and of operating costs.

Recently a canadian steel-manufacturing company contacted IMRI to inquire about the possibility of using a number of optical proximity sensors to monitor the position of the steel sheet in a hot-dip galvanizing line. A diagram of the galvanizing process is shown in Fig. 18. The steel sheet is drawn up from a bath of molten zinc at a speed of the order of 1 m/s. A couple of air knives is placed a few inches above the molten-zinc pool to reduce the thickness of the molten zinc film through the pressure of an air-blown curtain on both sides of the sheet. The exerted pressure, and thus the residual thickness of the zinc coating, is strongly dependent upon the distance between the air knife and the steel sheet. If the sheet is closer to one of the air knives, the higher pressure on that side will result in a coating thickness inferior to the specifications, while an excess of expensive zinc will be coated on the opposite side. Similar considerations are valid if the sheet is not perfectly parallel to the knives. A series of range-sensing devices, as shown in Fig. 1, would allow to continuously control the sheet position for a continuous control of the galvanizing process.

The best known optical approach for close-distance ranging is based on triangulation, whose principle is shown schematically in Fig. 19. A laser beam is projected on the inspected surface, and the position of the light spot is imaged by a camera at an angle. The distance of the surface can be evaluated from the position of the imaged spot on the camera retina.

A number of problems make such a technique inadequate for practical applications in the industrial environment. The apparatus is relatively bulky while the laser and camera electronics cannot withstand the strong mechanical shocks or the high-temperature environments which are often found in the industrial production lines. The range of measurement is relatively small: the image of the light spot on the camera retina goes out of focus for large excursions of the workpiece, while a reduction of the lens aperture coupled to signal interpolation techniques across the camera image in order to increase the depth of field lead to large inaccuracy because of an increase of the random laser-speckle noise. Finally, the normal-projection configuration cannot be used in the case of shiny surfaces because of signal-fading problems.

The range monitoring approach which is under development at our institute is shown in Fig. 20. The device comprises a rugged sensor head, which is installed close to the workpiece surface whose distance is to be monitored, and a remote power unit, containing the delicate

light source, detection, and signal-processing electronics which are safely kept at a distance from the hostile production-line environment. The two units are connected through a heavy-duty cable typically 10 m-long.

An important aspect of the described approach is the increased depth of field which can be obtained by proper orientation of the fiber-array image plane. As shown in Fig. 20, the fiber-optic linear array on which the image of the projected light spot is formed is oriented at an angle such that the intersection of the line-array direction and of the central plane of the collecting lens coincides with a point situated on the axis of the projected light beam. This insures that the imaged spot will be well in focus for any position of the surface, as will be shown in the appendix. This results in a uniformly sharp sensitivity over the full range of surface positions, as demonstrated in Appendix 1.

An open-box view of the sensor head is shown in Fig. 21 during laboratory calibration using a travelling mirror. During the preliminary tests, a position sensing detector was inserted directly in the fiber-array plane. Because of the symmetry of the light projecting and viewing directions with respect to the surface normal, this device can be used to monitor both shiny and matt-finish surfaces. A calibration signal is shown in Fig. 22. An acceptable linearity is obtained over the $\pm$ 2 cm depth range with a surface displacement accuracy of the order of 0.1 mm.

Some preliminary tests of the sensor were made on the IMRI steel-galvanizing pilot line operated in a closed loop without molten zinc. A comparison was made between the output from the optical sensor and the output from an LVDT probe contacting the sheet through a small wheel. The setup is shown schematically in Fig. 23a. Chart-recorder traces of the two outputs while the sheet was periodically displaced by a few mm are shown in Fig. 23b (the two traces were slightly shifted in the vertical direction for better comparison). The two signals are consistent in general, but the small high-frequency vibrations are not followed by the LVDT device because of the damping effect of the rubber wheel. It should also be mentioned that, in contrast with the calibrating curve of Fig. 22, which was recorded with a mirror-like reflecting surface, the pilot-line tests shown in Fig. 23 were obtained with a diffuse steel-sheet surface, showing that the optical sensor operates as well for the inspection of diffuse or specular surfaces.

CONCLUSION AND ACKNOWLEDGEMENTS:

Optical techniques appear to have a large and relatively unexploited potential for on-line industrial inspection. Their remote-sensing capabilities, as well as the recent availability of rugged, inexpensive, and reliable optoelectronic components, make optical devices an attractive tool whose in-process applications are expected to grow significantly in the years to come.

The authors wish to thank S. Golden, L. Charpentier and C. Archambault, of Union Carbide, as well as J. Kao of Reynolds Aluminum and P. Leclair of Emballages St-Jean for assistance during the in-plant trials of the film thickness prototype. Numerous interactions with T.R. Siack of Stelco for the analysis of the steel roughness monitoring device are deeply appreciated. Finally, advice and assistance from B. Champagne and H. Levert of our institute for the trials of the range-monitoring device is gratefully acknowledged.

APPENDIX

We demonstrate here that the projection of the line along which the image of the light spot moves as the workpiece surface is displaced intersects the central plane of the collecting lens on a point situated along the axis of the projected beam.

With reference to Fig. A-1, let us suppose that the above statement is not true, i.e. that $h \neq h'$. By differentiating the lens-imaging formula:

$$\frac{1}{s} - \frac{1}{s'} = \frac{1}{f}$$

We obtain:

$$\frac{\Delta s}{\Delta s'} = \frac{s^2}{s'^2} \qquad \text{(A-1)}$$

On the other hand, using the relation between similar triangles in Fig. A-1, we can write:

$$\frac{L'}{L} = \frac{s'}{s} \qquad \text{(A-2)}$$

From the trigonometric properties of the right-angle triangle in Fig. A-1, we can also state:

$$h' = \frac{s'}{\tan \alpha'} = \frac{s'L'}{\Delta s'} \qquad \text{(A-3)}$$

and:

$$h = \frac{s}{\tan \alpha} = \frac{sL}{\Delta s} \qquad \text{(A-4)}$$

from which we obtain:

$$\frac{h'}{h} = \frac{s'L'\Delta s}{s\ L\ \Delta s'} \qquad \text{(A-5)}$$

or, using equations (A-1) and (A-2):

$$\frac{h'}{h} = \frac{s'}{s}\ \frac{s^2}{s'^2}\ \frac{s'}{s} = 1 \qquad \text{(A-6)}$$

as it was to be shown.

REFERENCES:

1. R.K. Miller, "3D Machine Vision" SEAI, Madison, GA and Technical Insights, Ft. Lee, N.J. (1985).

2. E.P. Papadakis, "Future growth of NDE" Mater. Eval., vol. 41, p. 1130 (1983).

3. P. Cielo (editor) "Optical Techniques for Industrial Inspection", Proc. SPIE, vol. 665 (1986).

4. T.M. Cardis, "Process FTIR analysis of a chlorofluoromethane stream", Proc. ISA Adv. Instr., p. 1215 (1986).

5. R.E. Schirmer, "On-line, fiber-optic-based near IR absorption spectrophotometry for process control", Proc. ISA Adv. Instr., p. 1229 (1986).

6. J.D. Lenk, (1980). Handbook of Controls and Instrumentation. Prentice-Hall, New York.

7. A. Von Hassel, (1985). "What's new in thickness gauging? Coextrusion and lots more". Plastics Technology, 31(2), pp. 71-78.

8. R.F. Edgar and P.H. Hindle, "Infrared absorption gauging-the future" in: "Optical Techniques for Industrial Inspection", P. Cielo editor, Proc. SPIE vol. 665, p. 101 (1986).

9. P. Cielo, K. Cole and B. Favis, "Optical inspection for industrial quality and process control", 6th IFAC Conf., Akron, OH, Oct. 27-29 (1986).

10. P.W. Kiedron, (1986). "Removing interference fringes to improve accuracy of film-thickness spectroscopic measurement", in Optical Techniques for Industrial Inspection. Proc. SPIE, vol. 665, p. 110 (1986).

11. P. Cielo, G. Vaudreuil and M. Dufour, "Surface roughness monitoring for industrial quality control" OE-LASE, Los Angeles, Jan. 12-14, 1987.

12. P. Beckmann and A. Spizzichino, "The scattering of electromagnetic waves from rough surfaces" Pergamon Press, Oxford, (1963).

13. T.V. Vorburger and E.C. Teague, "Optical techniques for on-line measurement of surface topography" Precision Engineering, vol. 3, p. 61 (1981).

14. D.J. Whitehouse, "Instrumentation for measuring finish, defects and gloss" Measurement and Effects of Surface Defects and Quality of Polish, L.R. Baker and H.E. Bennet editors, Proc. SPIE, vol. 525, p. 106, (1985).

15. R. Brodmann, O. Gerstorfer and G. Thurn, "Optical roughness measuring instrument for fine-machined surfaces" Opt. Eng., vol. 24, p. 408, (1985).

16. Y. Shibata, Y. Asano, K. Kurita, and M. Shiozumi, "On-line glossmeter for stainless steel sheets" Optical Techniques for Industrial Inspection, P. Cielo editor, Proc. SPIE vol. 665, p. 25, (1986).

17. T.C. Strand "Optical three-dimensional sensing for machine vision" Opt. Eng., vol. 24, p. 33 (1985).

18. R. Pirlet et al., "Optical systems for dimensional control in hostile environments", P. Cielo editor, Proc. SPIE vol. 665, p. 61, (1986).

19. H. Denstman "State-of-the-art optics: automated image focusing", Ind. Phot., July 1980, p. 33.

20. N.J. Harrick, (1971), "Determination of refractive index and film thickness from interference fringes". Appl. Opt., 10, pp. 2344-2351.

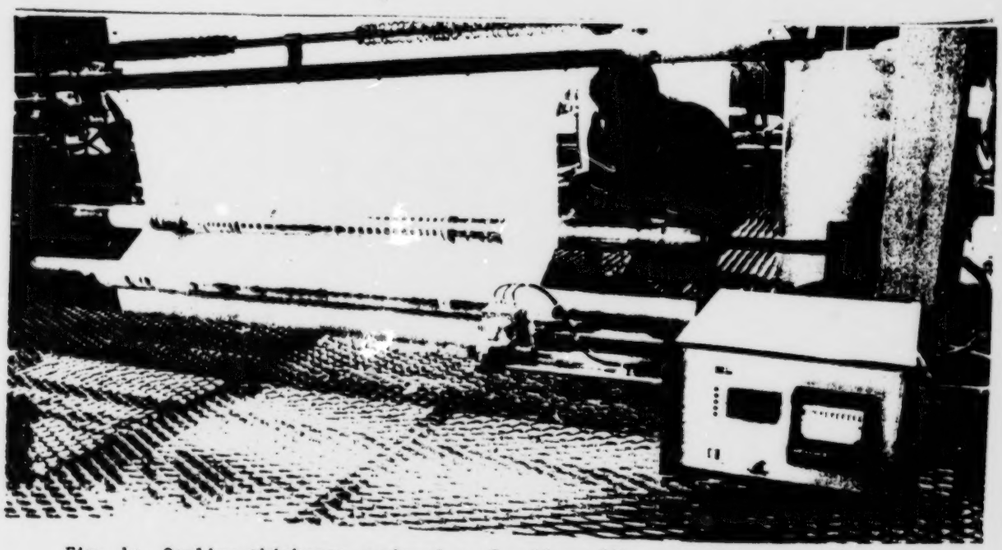

Fig. 1: On-line thickness monitoring of a blown-film extruded polyethylene sheet.

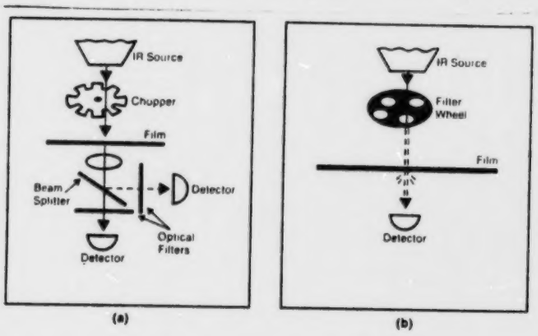

Fig. 2: Typical infrared-absorption configurations for monitoring film-thickness by (a) simultaneous comparison of transmissivity of two wavelengths and (b) sequential analysis of spectral transmissivity.

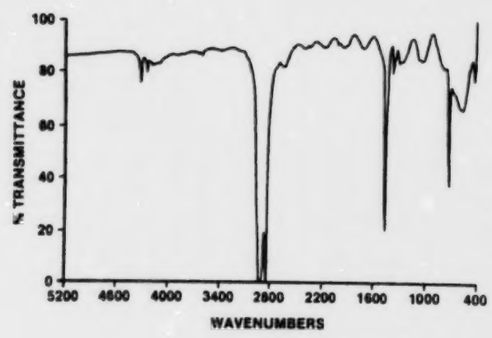

Fig. 3: FTIR spectral scan of light transmitted through a 15 μm-thick polyethylene film.

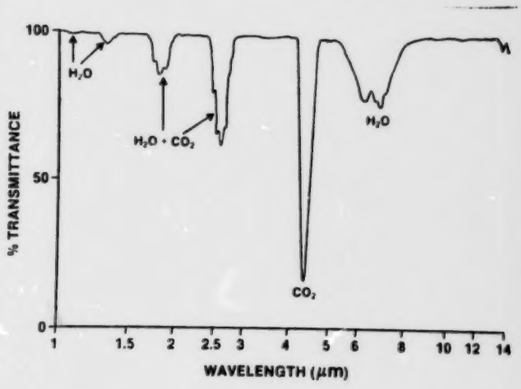

Fig. 4: Infrared transmission through 1 m of air at standard conditions.

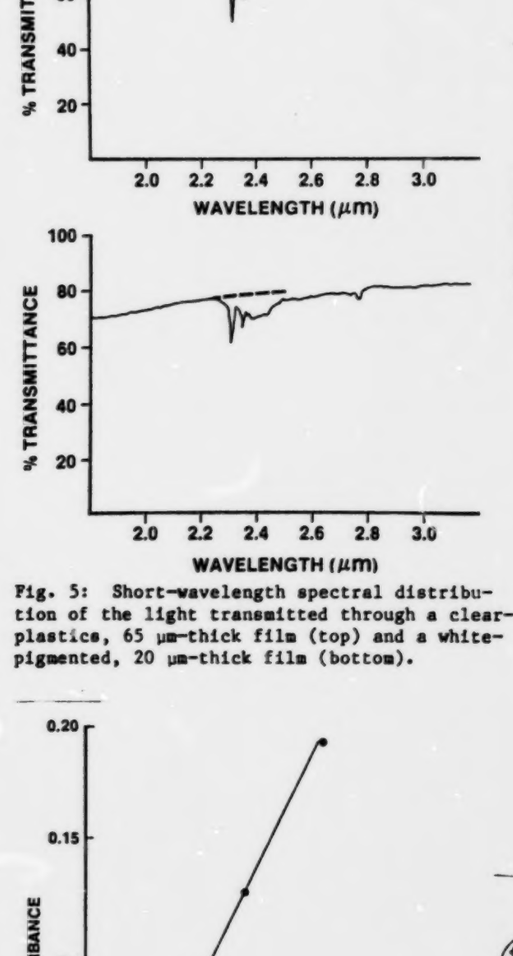

Fig. 5: Short-wavelength spectral distribution of the light transmitted through a clear-plastics, 65 μm-thick film (top) and a white-pigmented, 20 μm-thick film (bottom).

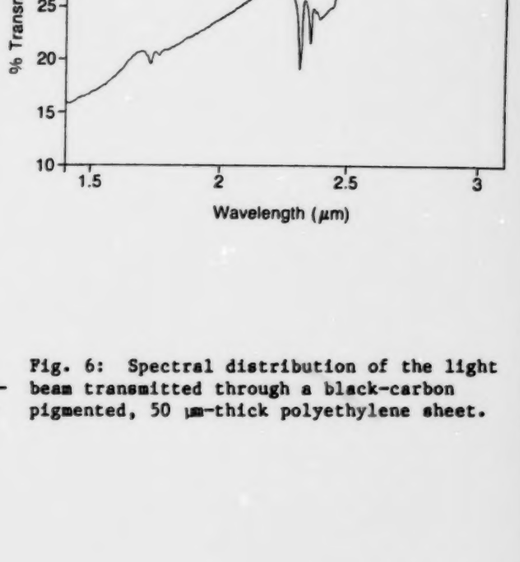

Fig. 6: Spectral distribution of the light beam transmitted through a black-carbon pigmented, 50 μm-thick polyethylene sheet.

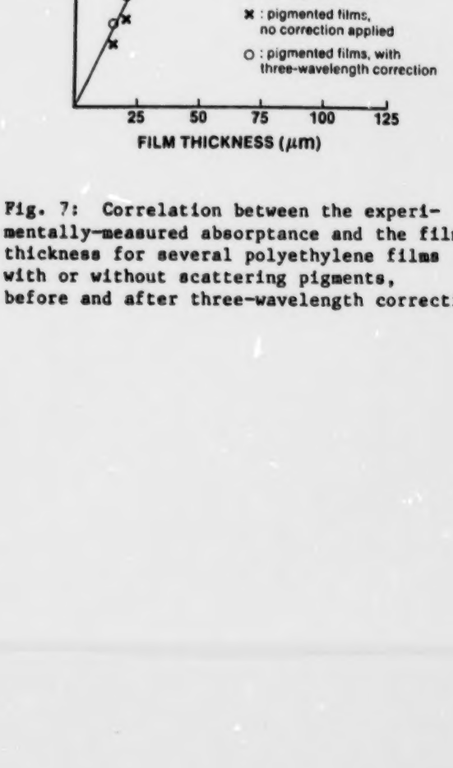

Fig. 7: Correlation between the experimentally-measured absorptance and the film thickness for several polyethylene films with or without scattering pigments, before and after three-wavelength correction.

Fig. 8: Setup for coating thickness measurement.

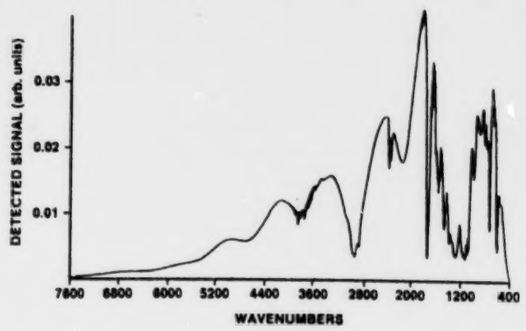

Fig. 9: Spectral distribution of the light reflected from a steel sheet with a 4.75 μm-thick polymeric coating at 57° incidence.

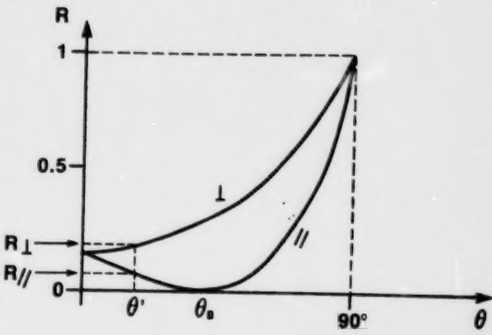

Fig. 10: Fresnel reflectivity vs. angle of incidence at an air-plastics interface, for light polarized in a direction parallel or perpendicular to the plane of incidence.

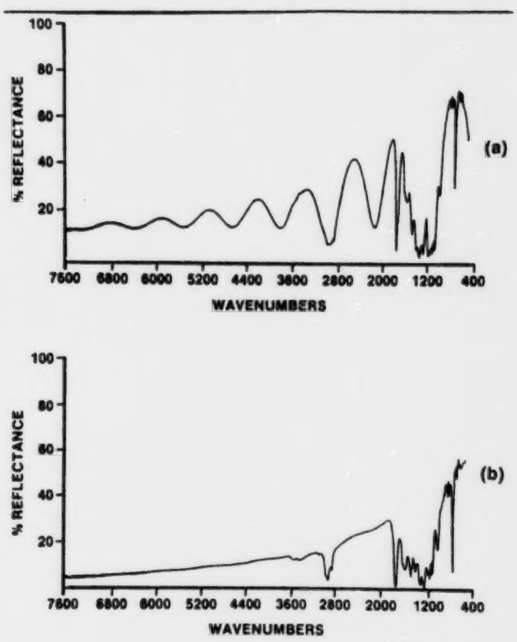

Fig. 11: Spectra obtained with the same sample as for Fig. 9 but using light polarized in a direction (a) perpendicular and (b) parallel to the plane of incidence. The spectra were normalized through division by the respective neutral-mirror reference curves.

Fig. 12: Surface structures of differently processed, galvanized-steel sheets with spangle of larger (a) and smaller (b) size, as well as of a sheet after temper-rolling (c) with spangle boundaries still visible.

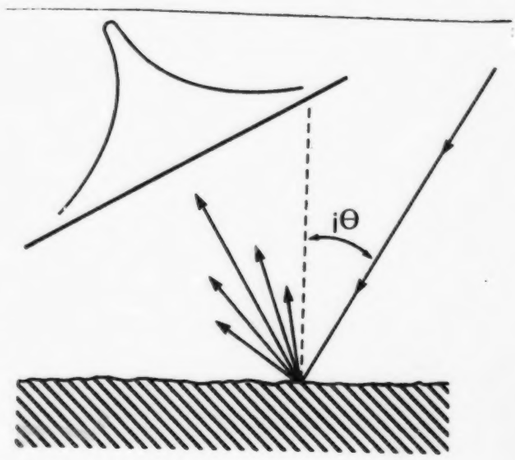

Fig. 13:

Scattering of light by a rough surface.

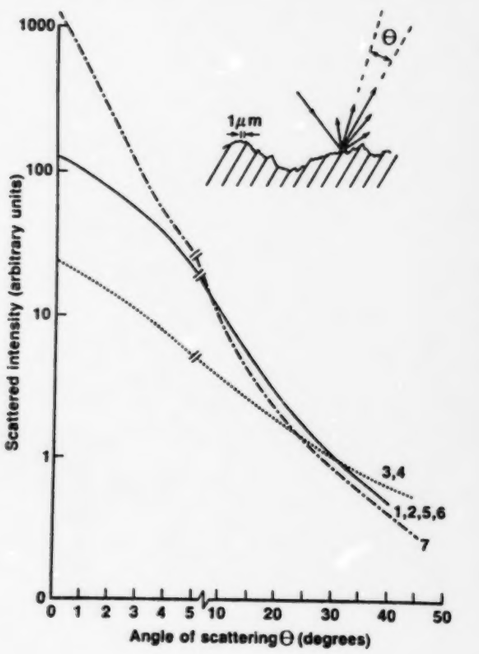

Fig. 14: Angular patterns of the scattered light from different galvanized-steel samples using a He-Ne laser.

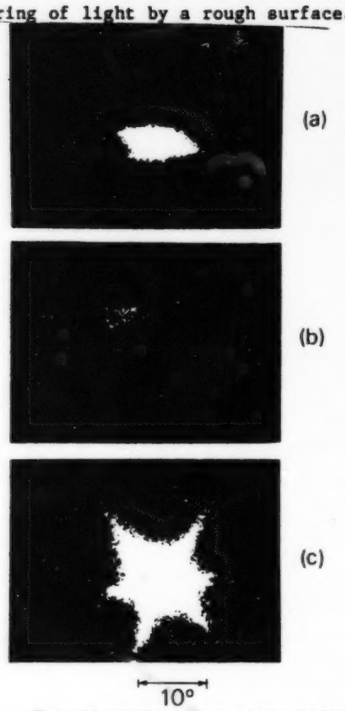

Fig. 15: Two-dimensional scattered-light patterns obtained in a (a) specular region, (b) matt-finish grain and (c) at the boundary between two grains.

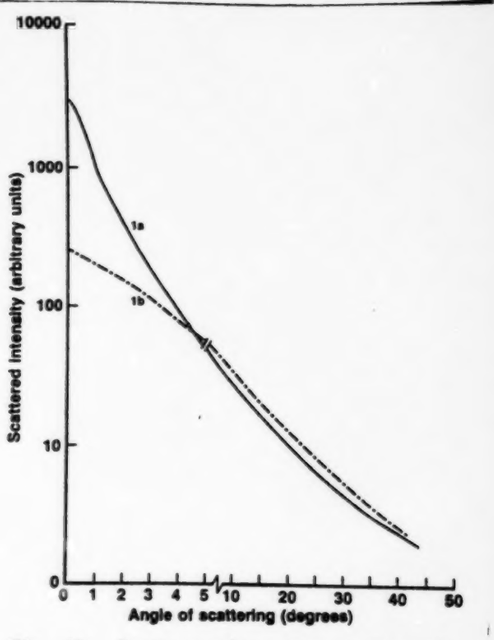

Fig. 16: He-Ne angular pattern of sample with conventional large-grain spangle in a specular (curve 1a) or matt-looking (curve 1b) grain region.

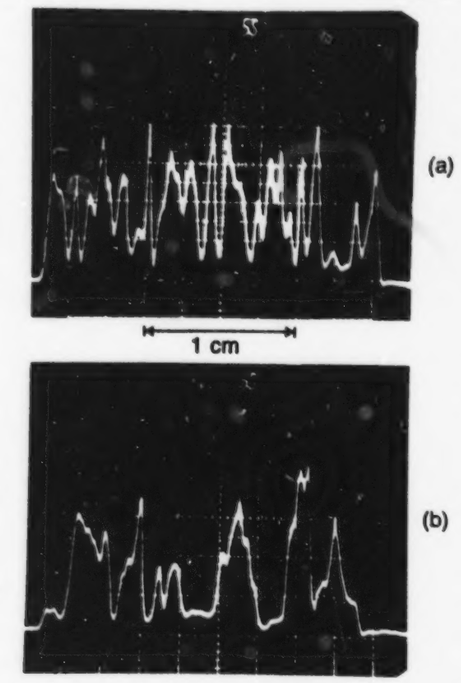

Fig. 17: Small-aperture scanned-specular-reflectivity signals obtained in a region with (a) spangle grain size ≈ 1 mm, (b) spangle grain size ≈ 3 mm.

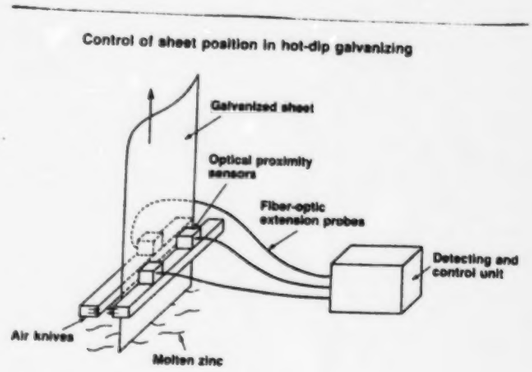

Fig. 18: Diagram of the hot-dip galvanizing process with proposed location of the optical proximity sensors.

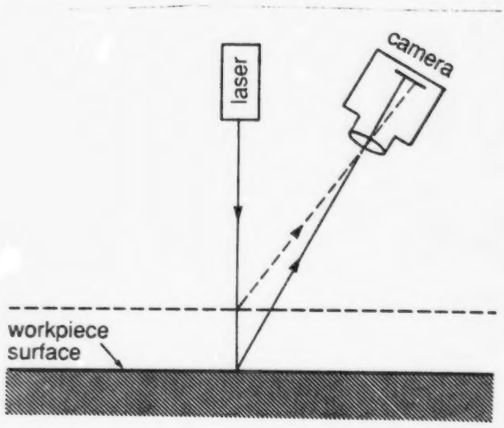

Fig. 19: Optical triangulation ranging (Prior art).

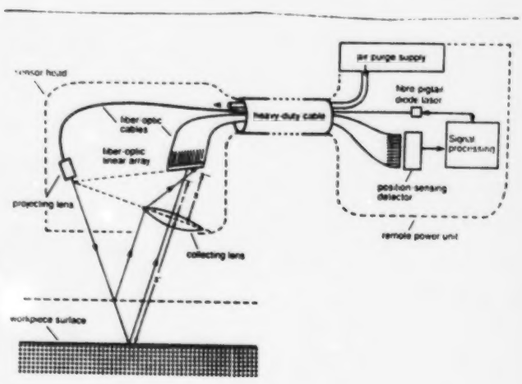

Fig. 20: Schematic diagram of the ranging device.

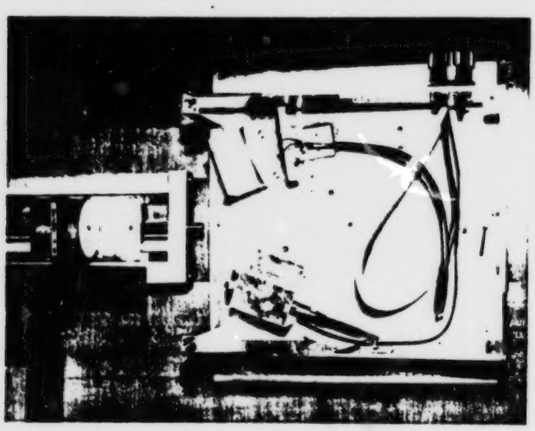

Fig. 21: Open-box view of the sensor head prototype during the laboratory calibration.

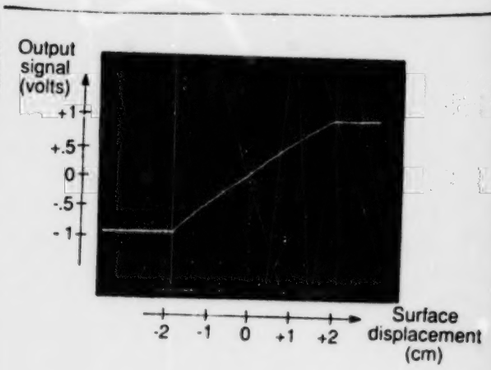

Fig. 22: Recorded calibration curve of signal output vs. surface displacement.

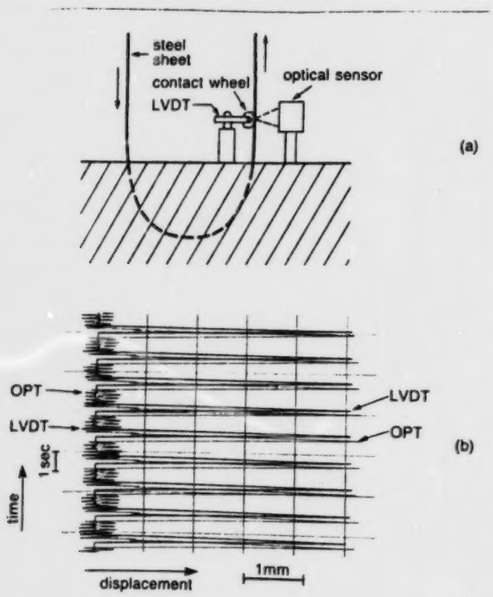

Fig. 23: Comparison of the performance of a contact device and of the optical sensor in the IMRI steel-galvanizing pilot line;
(a) experimental setup;
(b) chart-recorder outputs from the two sensors (the traces are purposely shifted laterally for better viewing).

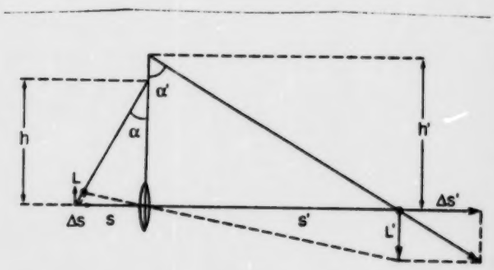

Fig. A-1:
Demonstration of the h - h' condition